Control of the Corrosion of Magnesium for Implant Application by Hydrothermally Deposited Biodegradable Calcium Phosphate Coating

Sara Kaabi Falahieh Asl[a,b], Sandor Nemeth[b*] , Ming Jen Tan[a]

[a] Nanyang Technological University, School of Mechanical & Aerospace Engineering

50 Nanyang Avenue, Singapore 639798

[b] Singapore Institute of Manufacturing Technology

71 Nanyang Drive, Singapore 638075

* Corresponding author. E-mail address: sandorn@SIMTech.a-star.edu.sg

Telephone: 65 6793 8374

Abstract

The corrosion protection of hydrothermally deposited calcium phosphate coatings on AZ31 magnesium alloy was studied for their potential use in biocompatible and bioresorbable temporary implants. The coating mainly consisted of calcium phosphate phases (monetite and tricalcium phosphate). Potentiodynamic and electrochemical impedance spectroscopy (EIS) confirmed that the coatings provided varying levels of corrosion protection depending on the coating deposition temperature and duration. EIS results showed that the size of capacitance loops and the absolute impedance value (|Z|) increases by increasing the deposition temperature and corresponding growth in coating thickness. In agreement with the electrochemical experiments, immersion tests in simulated body fluid also indicated large improvement in corrosion protection as the mass loss was significantly reduced when coating was applied as compared to the bare metal. Using the thickest coating obtained at 190 °C deposition temperature, the corrosion current density of the coated magnesium was 10,000 fold lower compared to the bare metal. This result confirmed that the new hydrothermal coating is suitable

to protect Mg implant against corrosion with further advantage of being bioactive and biodegradable.

Keywords: Biomaterials, coatings, corrosion, corrosion test, electrochemical techniques, electrochemical properties.

1. Introduction

The interest in using magnesium alloys has been steadily increasing [1-3] due to their low density and favorable mechanical properties. However, a significant obstacle of using magnesium in most applications is its rapid corrosion requiring corrosion protection measures. One of the emerging applications of magnesium is its use as biocompatible and biodegradable temporary implant material [2, 4], when its corrosion is taken advantage of by allowing the magnesium metal to corrode and be absorbed by the body. Magnesium could provide significant advantage compared to currently used implants made of titanium (Ti), stainless steel (S.S.), and cobalt-chromium (Co-Cr) alloys when used for temporary implantation since it does not require removal and associated second operation. Magnesium alloys are also advantageous in reducing the stress shielding effect due to the mismatch in mechanical properties between implant materials and bone tissue. The stress shielding phenomenon causes stress concentration at bone-implant interfaces and may result in critical clinical issues such as implant loosening, delay in healing process and consequently damaged bone growth. Ti, SS, and Co-Cr alloys have high Young's modulus (100–200 GPa) while magnesium alloys have lower modulus (41-45GPa), close to that of human bone (10–30 GPa); therefore use of Mg avoids or minimizes stress shielding effect [2, 4, 5].

Despite the high potential of using magnesium alloys as temporary and biodegradable implants, applications are not widespread as the corrosion rate of Mg alloys is too high, resulting in excessive hydrogen evolution and local alkalization close to the surgery region, as well as premature degradation in the implant's mechanical integrity before sufficient bone healing can occur[6]. To put Mg to practical use, it is necessary to improve its corrosion performance through alloying or surface modification. Although the corrosion resistance of Mg can be enhanced by alloying elements with low toxicity such as zinc and calcium, the amounts of these elements must be limited in order to maintain desired mechanical properties and reduce potential toxicity leading to insufficient improvement in corrosion properties. The alternative is surface modification and coating that could reduce the corrosion rate to a higher extent [7, 8]. Anodizing, electrodeposition, fluoride conversion and biomimetic coatings have been used on Mg alloys. However, these coatings do not provide sufficient protection: Biomimetic and anodic coatings are reportedly rather permeable, exhibiting many cracks [1, 9]. Relatively thin but dense coating can be made of magnesium fluoride (MgF_2) as a conversion coating but it gradually dissolves when the sample is transferred to fluoride-free solutions; precluding long-term protection [1, 9].Thus, no suitable coating seems to exist for magnesium implant application and there is a need for a novel coating that is dense and able to provide superior corrosion protection. In addition, the coating must be biodegradable and biocompatible as the biological response of implant materials strongly depends on the implant's surface properties due to interactions between the cells and biomaterials taking place at the tissue-implant interface [10].

For biomedical applications calcium-phosphate (Ca-P) coatings are preferred since Ca-P is the main inorganic constituent of natural bone and it can speed up bone growth. Producing Ca-P crystals by hydrothermal process has a successful history [11-15]. However, there are only a few

publications regarding deposition of Ca-P crystals directly on metal substrate. Liu et al. reported deposition of a fairly uniform crystalline hydroxyapatite (HA) layer on metal substrates by seeded hydrothermal deposition method in two steps: Deposition of a seed layer by means of electrochemical method which was followed by hydrothermal process. They found that the seed layer improves the deposition of HA layer during hydrothermal process. However, they did not investigate the corrosion performance of the obtained coatings [16]. Onoki et al. used a double layered capsule hydrothermal hot-pressing technique for developing HA coating on Ti and Mg substrates with good adhesion properties (4-5.5 MPa) [17, 18]. Hiromoto et al. used hydrothermal method to deposit HA in a wide range of pH, and they reported 10-foldimprovementin the corrosion performance of Mg substrate but this is not fully adequate for protecting Mg substrate in implant application. Ng et al.[19] and Zhu et al.[20]developed a thick magnesium hydroxide layer, $Mg(OH)_2$, by means of hydrothermal process for surface modification of Mg. Gupta et al. developed compact and pore-free $Mg(OH)_2$layer which improved corrosion performance of Mg substrate in phosphate buffer saline (PBS) solution [21].Although, $Mg(OH)_2$ layer can improve the corrosion performance of Mg substrate it is not preferred in biomedical application unlike the biodegradable and biocompatible Ca-P coatings. Apart from biocompatibility requirement, the deposited coating layer must be dense and adherent. Thus, a hydrothermal deposition method was selected in the present work to grow bioresorbable Ca-P coating in such a way that most of the coating defects would undergo self-healing during the deposition and thus provide high corrosion resistance.

The hydrothermally deposited Ca-P coating was successfully prepared and partially characterized for its composition and mechanical properties as reported separately [22]. XRD analysis showed that the deposits obtained from hydrothermal process were mainly a mixture of

monetite ($CaHPO_4$) and tricalcium phosphate with small amount magnesium substitution [$Ca_{2.86}Mg_{0.14}$ $(PO_4)_2$, also known as whitlockite]. Similarly, the FTIR spectra for Ca-P coating layers deposited showed vibration bands corresponding to monetite and tricalcium phosphate phases.

Moreover, the coating thickness was found to increase slightly by increasing the deposition temperature from 100 ºC to 160 ºC (from 20 µm to almost 60 µm) followed by a sharp increase to around 400 µm at 190 ºC. With the increase in coating thickness the coating adhesion dropped from 5.8 MPa (sample coated at 160 ºC) to 3.1MPa (sample coated at 190 ºC).The investigation of corrosion behavior of the coated magnesium alloy by electrochemical methods is reported in this work.

2. Experimental details

2.1. Materials

The hydrothermal coating deposition method was reported elsewhere [22], using analytical grade $Ca(NO_3)_2$ (99.98% purity) and $NH_4H_2PO_4$ (98% purity), obtained from Alfa Aesar. AZ31 magnesium alloy was used as substrate for the coating process. Disks were prepared with 25 mm diameter and 2 mm thickness from commercial AZ31 rod. Prior to coating process, AZ31 substrate was prepared with up to 2400 grit abrasive paper, and then ultrasonically cleaned in acetone for 20 minutes prior to coating.

The coated samples were named as HE100 ºC-3hr and HE130 ºC-3hr, HE160 ºC-3hr and HE190 ºC-3hr respectively, referring to the deposition temperature and duration. For the 190 ºC hydrothermal process, heating durations of 1and 2 hours were used as well.

2.2. Characterization of coatings

The electrochemical behavior of uncoated and coated samples was investigated by potentiodynamic polarization test using a Solarton potentiostat (Model SI 1287) conducted in simulated body fluid solution (SBF) according to a reported procedure [23] at pH 7.2-7.4. For the electrochemical tests, a three-electrode cell was used with the sample as working electrode, SCE (sat. KCl) was used as the reference, and graphite as the counter electrode. An area of 1 cm^2 of the working electrode was exposed to the solution. A 1 mVs^{-1} scanning rate was applied during the potentiodynamic polarization test. Prior to the polarization test, samples were equilibrated in SBF solution for 30 minutes.

Electrochemical impedance spectroscopy (EIS) test was performed in order to investigate the corrosion behavior of coatings in SBF solution using a Solarton potentiostat (Model SI 1260). The EIS tests were conducted at the open circuit potential (OCP) in the frequency range of 100 kHz to 10 mHz, using 10 mV amplitude of signal's perturbation.

Immersion tests were conducted in SBF standard solution for up to 28 days in order to assess the early corrosion performance. Each sample with an exposure area of 4.9 cm^2 was immersed in 50 ml of the SBF solution at 37 ºC. After each immersion time, the samples were extracted and the corrosion products were removed by using chromic acid and silver nitrate according to the method described in the literature [24]; then the samples were cleaned with ethanol and dried. Finally, the sample masses were measured.

After each immersion period in SBF solution, 5 ml of solution was extracted and analyzed by using an inductively coupled plasma atomic emission spectrometer (ICP-MS7700, Agilent) in

order to determine the Mg ion release from the samples during the immersion periods. The changes in pH value of the SBF solution with uncoated and coated samples were monitored overtime as well. For the immersion test and ion release measurements, the reported results are the means of triplicate measurements and the data are reported as mean ± standard deviation.

3. Result and discussion

3.1. Electrochemical test results

Electrochemical measurements were done in SBF solution to characterize the corrosion performance of the samples by means of open circuit potential (OCP) and potentiodynamic polarization. The variation of OCP over time can be used as a criterion to understand the interface stability of coating and substrate. OCP curves for uncoated and coated samples are illustrated in Fig.1.a. The OCP of the coated samples shifted to nobler potential as compared to the bare alloy. The OCP of coated sample deposited at 190 ºC increased by 1.72 V compared to AZ31 bare substrate while 1.22 V increase was seen for coated sample at 160 ºC. The positive shift of OCP due to the presence of coating indicates the formation of a stable Ca-P/AZ31 interface [25, 26].The much nobler behavior of the coated sample at 190 ºC and the stable OCP over a 30 minutes period can be attributed to the improved stability of the coated alloy surface that may be related to high coating thickness and more complicated paths of electrolyte penetration into coating layer due to its compact morphology. The observations indicated that Ca-P layer has a protective nature and could provide good protection for Mg substrate.

Fig.1.b and Fig.2 show the potentiodynamic curves for coated samples deposited at different temperatures for three hours and coated samples deposited at 190 ºC for different deposition

times, respectively. The corrosion potential (E_{corr}) and the corrosion current densities (j_{corr}) were derived from the polarization curves by means of Tafel extrapolation method, and the results are summarized in Table1. According to the data, the corrosion rate of coated samples decreased significantly compared to the uncoated sample. The corrosion rate was reduced by increasing the hydrothermal deposition process temperature. This was likely due to an increase in the coating thickness and changes in coating morphology. The corrosion resistance of Mg substrate was enhanced approximately 10,000-fold after coating at 190 ºC.

Mg and its alloys suffer from pitting corrosion (as it observed from the SEM image after corrosion test, but these results were not shown here) manifesting in rapid increase in the anodic current over small polarization potential range in potentiodynamic scans which can be seen clearly in Fig. 1.b for the bare substrate and coated sample at 100 ºC. On the other hand, samples coated at 130 ºC and 160 ºC, the polarization curves show an abrupt increase in anodic current followed by a quasi-passive region at around 10^{-5} A/cm^2, while in the case of the coated sample at 190 ºC it only had a quasi-passive region in polarization curve at around $5*10^{-7}$A/cm^2.

The change in corrosion rate of coated sample at 190 ºC was examined for different deposition durations from 1 to 3 hrs, as shown in Fig.2. By increasing the deposition time, the protective nature of the coating improved, probably due to the increase in coating thickness and formation of a more compact morphology.

The corrosion improvement can be better understood by considering the corrosion process of the metal. Mg reacts with SBF solution immediately upon contact and starts to corrode according to Eq's.1-3[27]:

$$Mg \rightarrow Mg^{2+} + 2e^{-} \qquad (1)$$

$$2H_2O + 2e^- \rightarrow H_2 + 2OH^- \quad (2)$$

$$Mg^{2+} + 2OH^- \rightarrow Mg(OH)_2 \quad (3)$$

The presence of a coating layer can prevent or delay the access of electrolyte to the Mg substrate and retard the initiation of corrosion process by limiting the availability of water needed for hydrogen generation according to Eq. 2. Thus, by increasing the coating thickness and improving the coating morphology, the corrosion rate can be decreased[26].

3.2. Electrochemical impedance spectroscopy (EIS) results

EIS measurements were done to understand the corrosion behavior and corrosion performance of coated and uncoated substrate in SBF solution. EIS measurements were analyzed by two methods: Nyquist impedance spectroscopy and Bode graphs for the bare and coated samples as given in Fig.3and Fig.4, respectively. It was clearly observed that the Nyquist graph for bare sample composed of two capacitive semi-circuits at medium and low frequency, followed by an inductive loop at low frequency region. The Bode phase graph of bare sample showed two phase maxima at low and medium frequency. The time constant at medium frequency can be attributed to the partially protective oxide layer and semi-circle at low frequency might be related to the charge transfer resistance (R_{ct}) and double layer capacitance (C_{dl}) at the surface of substrate [28]. The calculated results from EIS graphs are reported in Table 2. The appearance of inductive loop at low frequency is probably due to film weakening and pit incubation. Coated samples at 100 ºC, 130 ºC and 160 ºC only showed a capacitance loop at medium frequency .The capacitive loop at medium frequency might be attributed to the coating layer polarization resistance (R_p).

The calculated capacitances for these time constants were in the range of 4-12 μF. Since the double layer capacitance is normally between 20-50 μF [29], the appearance of this semi-circle is related to coating layer resistance. The size of capacitance loops was increased by increasing the deposition temperature. This is in parallel to the increase in charge transfer and polarization resistance which is a criterion for corrosion resistance enhancement[30].

The coated sample at 190 ºC showed a different behavior. For the coated samples at 190 ºC, the Nyquist graph was composed of two capacitive loops at high and medium frequency. The high frequency time constant can be related to coating layer resistance and the presence of capacitive loop at medium frequency range can be related to the new surface formation at the electrode surface as a result of partial delamination of top surface of coating[31]. This result is in agreement with the potentiodynamic test data. According to Fig1.a and Fig1.b, there is a big difference between the OCP value for the coated sample at 190 ºC and its corrosion potential. Normally the values of these two potentials are close. However, the formation of a new surface during corrosion process can result in the shift of these potentials.

Since the coating made at190 ºC was the thickest (400μ), the high thickness might result in increased residual stress and delamination of the top layer of coating resulting in the emergence of the second capacitive loop at medium frequency range. However, for the coated sample at190 ºC, the diameter of capacitive loop at medium frequency, was significantly larger than that of other coatings, which confirmed that this coating possesses higher corrosion resistance compared to other coatings.

From the Bode plot (Fig.4.b), it is obvious that coated substrates have larger impedance (|Z|) values compared to the bare substrate, which means the corrosion performance of coated sample is much better than bare substrate [26]. The absolute impedance value (|Z|) increases by increasing the deposition temperature. The EIS results are thus in good agreement with potentiodynamic results and confirmed that by increasing deposition temperature, the corrosion performance of coated samples improved.

The impedance data for the bare and coated samples were fitted to theoretical models as shown in Fig.5. For the bare substrate, C_f is considered as oxide film capacitance, while in the case of the coated sample it is related to the coating layer capacitance. C_{ns} is related to the newly formed surface at the surface of coated sample at 190 ºC. R_p and R_{pns} represent the coating layer and newly formed surface polarization resistance respectively. R_{ct} represents the charge transfer resistance at the surface of substrate and C_{dl} shows the double layer capacitance at the surface of electrode and L represents an inductance. The fitting results were in good agreement with the original impedance graphs.

3.3. Mass loss of samples during immersion test

The mass loss is a common test for evaluating corrosion performance as reported in literature [32, 33]. In this study the mass loss of bare and coated magnesium samples was monitored during immersion in SBF solution as shown in Fig.6. As soon as Mg is immersed in the SBF solution corrosion takes place which results in the release of hydrogen gas and consequently formation of magnesium hydroxide, $Mg(OH)_2$, on the surface of Mg according to Eq.3. Since SBF solution contains aggressive ions such as chloride (Cl^-), the $Mg(OH)_2$ layer can convert into

soluble $MgCl_2$ according to Eq.4 [34]. The soluble $MgCl_2$ cannot protect the surface of Mg and consequently, the mass loss of the sample increases as the immersion time becomes longer.

$$Mg(OH)_2 + 2Cl^- \rightarrow Mg(Cl)_2 + 2OH^- \quad (4)$$

The total mass loss from the uncoated AZ31 was 38.7 mg/cm^2 after 28 days immersion in SBF solution, while that of the coated samples were significantly lower. For example, samples coated at 160 ºC had mass loss of 14.32 mg/cm^2. In the case of samples coated at 100 ºC and 130 ºC, the mass loss after 28 days immersion in SBF solution was 27.29 mg/cm^2 and 21.38 mg/cm^2 respectively. This mass loss also included partial dissolution of the coating layer during the test. The degradation rate of the magnesium samples, as measured by mass loss, decreased 3-fold by applying the coating at 160 ºC, and the major part of weight loss for the coated samples was contributed by partial coating layer dissolution.

3.4. Surface morphology study after immersion test

Photographs of tested samples after 28 days immersion in SBF are shown in Fig.7. As it can be seen from the photographs, the uncoated Mg substrate undergoes severe and non-uniform corrosion after 28 days immersion in SBF solution. As immersion time increased, the pits on the surface of Mg became wider and started to penetrate through the substrate thickness (the photographs of other immersion times are not shown here). In some part of substrate pits propagated through the whole 2 mm substrate thickness leading to premature loss of mechanical integrity. On the other hand, the coated samples at 130 ºC and 160 ºC depositions displayed intact coating and no obvious pits were observed on the coating surface.

Since the Mg $(OH)_2$ layer is not protective and can transform into soluble $MgCl_2$, the breakdown of $Mg(OH)_2$ layer can provide more active sites which accelerates the corrosion of substrate. Moreover, the difference in electrochemical activities of different phases in Mg results in the formation of microcells and consequently galvanic corrosion can happen after dissolution protective layers resulting in the formation of a non-uniform corrosion process [34].

SEM images of the bare and coated samples after 28 days immersion test are shown in Fig.8. From the SEM micrograph it is clear that surface of Mg substrate undergoes severe corrosion and shows a rough appearance. However, in the case of coated sample at 160 ºC, the coating layer still remained on the surface of substrate but Ca-P crystals started to dissolve as some pits appear on the surface of the Ca-P crystals. Formation of pits on the surface of Ca-P crystals might be attributed to the dissolution of monetite. Monetite is a stable phase below pH value around 5. Since the pH was around 7.2-7.4 in the SBF solution, this higher pH could break down the thermodynamic equilibrium at the interface of monetite and solution and results in dissolution of monetite phase according to Eq.5 [35].

$$CaHPO_4 \rightarrow Ca^{2+} + HPO_4^{2-} \quad (5)$$

3.4. Ion release measurements and pH monitoring and evaluation of mechanical integrity

The ion release of uncoated and coated samples was measured by means of ICP techniques. The results are shown in Fig.9 and detailed in Table3. For the uncoated samples, the Mg ion release increased from 83 ppm/cm^2 after 2 days immersion to 174 ppm/cm^2 after 28 days immersion in SBF solution. The release of Mg ions from the coated sample was low compared to the uncoated

sample. In the case of coated samples at 160 ºC, the Mg ions release started from 11 ppm/cm^2 after 2 days of immersion and reaching 108 ppm/cm^2 after 28 days immersion in SBF solution. The results show Ca-P coating can protect Mg substrate from corrosion and can decrease the degradation rate of Mg substrate significantly.

Apart from Mg ion release, fast hydrogen evolution and consequently alkalization are critical issues resulting from corrosion of Mg that may delay the healing process and adversely affect new tissue formation and cell proliferation. To see if the present coatings can overcome this problem, the change in pH value over immersion time in SBF solution was monitored for uncoated and coated samples, and the result is shown in Fig.10. The initial measured pH value of the SBF solution was 7.35, and it increased significantly after one-day immersion to 8.4 and leveled out to 9.95 after 10 days immersion for uncoated sample. For the sample coated at 160 ºC, the change in pH (to 7.42) was minor after one-day immersion and increased to 8.35 after 10 days immersion. The results confirmed that the present coating can moderate the pH increase induced by Mg corrosion.

The presence of a coating layer acts as a barrier to prevent access of electrolyte to the substrate. By increasing the immersion time, the solution can penetrate through the coating via pits and the substrate dissolution and pH increase start. However, the changes in the pH values for the coated samples were much smaller than the bare substrate. This phenomenon might be explained by Eq.5 describing the dissolution of the coating.

As a result of dissolution of monetite phase, HPO_4^{2-} is released from the surface which can moderate the pH increase due to substrate dissolution. Moreover, during the immersion test in the SBF solution, monetite partially converts to hydroxyapatite (HA) through the dissolution-

reprecipitation mechanism. The dissolution of monetite at this slightly alkaline pH and concurrent precipitation of Ca^{2+} and PO_4^{3-} ions due to their high concentration in SBF solution leads to eventual thermodynamic equilibrium by the conversion of monetite into HA. The conversion may be described by Eq.6 [35]:

$$5Ca^{2+} + 3HPO_4^{2-} + OH^- \rightarrow Ca_5(PO_4)_3(OH) \qquad (6)$$

As it can be seen from Eq. 6 some OH^- ions are consumed during the formation of HA, which also helps to keep the solution pH from rising rapidly.

4. Conclusion

In the present report, corrosion performance of hydrothermally deposited Ca-P coatings on Mg substrate were evaluated and compared to bare Mg substrate for potential biomedical application. The Ca-P coatings consisting of a mixture of bioactive and resorbable monetite and tricalcium phosphate improved the corrosion performance of Mg substrate up to 10,000-fold as measured by the corrosion current density. EIS results showed that the size of capacitance loops increased after applying the coating layers on Mg substrate and the capacitance loop's size was increased by increasing the deposition temperature. This was in parallel to the increase in charge transfer and polarization resistance which is a criterion for corrosion resistance enhancement and confirmed the results from potentiodynamic tests. The coating evaluation indicated that the corrosion resistance improved by increasing deposition temperature due to deposition of thicker layer at higher temperature. However, EIS also revealed that coatings deposited at the highest temperature (190°C) did not behave the same way as coatings prepared at lower temperature as

new surface formation was indicated that suggests the delamination of coating top layer. This suggested that coating structure and deposition mechanism may change with changing deposition temperature. The presence of a coating layer can delay the access of electrolyte to the Mg substrate and retard the initiation of corrosion process by limiting the availability of water needed for hydrogen generation. Thus, by increasing the coating thickness and improving the coating morphology, the corrosion rate decreased. There appears to be an optimum deposition temperature at about 160 °C that can produce coatings with good corrosion protection and stability.

The hydrothermally deposited coating appears to be a viable protection layer for implant applications using magnesium substrates. In addition to high corrosion resistance, the degradation rate of coated magnesium can be readily adjusted by the variation of deposition temperature and deposition duration. Although the corrosion resistance of the coating appears to meet the implant application requirements, further study is needed to test in vitro performance in cell culture, as well as better understanding of deposition mechanism during hydrothermal process.

Acknowledgments

The authors would like to express their gratitude to Singapore Agency for Science, Technology and Research (A*STAR), Singapore Institute of Manufacturing Technology (SIMTech), and Nanyang Technological University for the financial support for this study.

References

[1] H. Hornberger, S. Virtanen, A.R. Boccaccini, Biomedical coatings on magnesium alloys - a review, Acta. Biomater 8 (2012) 2442.

[2] G. Song, S. Song, A Possible Biodegradable Magnesium Implant Material, Adv. Eng. Mater 9 (2007) 298.

[3] F. Witte, N. Hort, C. Vogt, S. Cohen, K.U. Kainer, R. Willumeit, F. Feyerabend, Degradable biomaterials based on magnesium corrosion, Curr. Opin. Solid State Mater. Sci 12 (2008) 63.

[4] F. Witte, The history of biodegradable magnesium implants: a review, Acta. Biomater 6 (2010) 1680.

[5] F. Witte, J. Fischer, J. Nellesen, H.A. Crostack, V. Kaese, A. Pisch, F. Beckmann, H. Windhagen, In vitro and in vivo corrosion measurements of magnesium alloys, Biomaterials 27 (2006) 1013.

[7] F. Witte, N. Hort, C. Vogt, S. Cohen, K.U. Kainer, R. Willumeit, F. Feyerabend, Degradable biomaterials based on magnesium corrosion, Curr. Opin. Solid State Mater. Sci 12 (2008) 63.

[8] J. Wang, J. Tang, P. Zhang, Y. Li, J. Wang, Y. Lai, L. Qin, Surface modification of magnesium alloys developed for bioabsorbable orthopedic implants: a general review, J. Biomed. Mater. Res. Part B Appl. Biomater 100 (2012) 1691.

[9] Y. Zhang, G. Zhang, M. Wei, Controlling the biodegradation rate of magnesium using biomimetic apatite coating, J. Biomed. Mater. Res. Part B Appl. Biomater 89 (2009) 408.

[10] N.T. Kirkland, N. Birbilis, M.P. Staiger, Assessing the corrosion of biodegradable magnesium implants: a critical review of current methodologies and their limitations, Acta Biomater 8 (2012) 925.

[11] A. Abdal-hay, M. Dewidar, J.K. Lim, Biocorrosion behavior and cell viability of adhesive polymer coated magnesium based alloys for medical implants, Appl. Surf. Sci. 261 (2012) 536.

[12] A.A. Chaudhry, J. Goodall, M. Vickers, J.K. Cockcroft, I. Rehman, J.C. Knowles, J.A. Darr, Synthesis and characterisation of magnesium substituted calcium phosphate bioceramic nanoparticles made via continuous hydrothermal flow synthesis, J. Mater. Chem., 18 (2008) 5900.

[13] W.L. Suchanek, K. Byrappa, P. Shuk, R.E. Riman, V.F. Janas, K.S. TenHuisen, Mechanochemical-hydrothermal synthesis of calcium phosphate powders with coupled magnesium and carbonate substitution, J. Solid State Chem. 177 (2004) 793.

[14] J.-K. Han, H.-Y. Song, F. Saito, B.-T. Lee, Synthesis of high purity nano-sized hydroxyapatite powder by microwave-hydrothermal method, Mater. Chem. Phys. 99 (2006) 235.

[15] T. Hattori, Y. Lwadate, Hydrothermal Preparation of Calcium Hydroxyapatite Powders, J. Am. Ceram. Soc 73 (1990) 1803.

[16] H.S. Liu, T.S. Chin, L.S. Lai, S.Y. Chiu, K.H. Chung, C.S. Chang, M.T. Lui, Hydroxyapatite synthesized by a simplified hydrothermal method, Ceram. Int. 23 (1997) 19.

[17] D. Liu, K. Savino, M.Z. Yates, Coating of hydroxyapatite films on metal substrates by seeded hydrothermal deposition, Surf. Coat. Technol. 205 (2011) 3975.

[18] T. Onoki, A. Nakahira, T. Tago, Y. Hasegawa, T. Kuno, Novel low temperature processing techniques for apatite ceramics and chitosan polymer composite bulk materials and its mechanical properties, Appl. Surf. Sci. 262 (2012) 263.

[19] T. Onoki, S.-y. Yamamoto, Hydroxyapatite ceramics coating on magnesium alloy via a double layered capsule hydrothermal hot-pressing, J. Ceram. Soc. Jpn. 118 (2010) 749.

[20] W.F. Ng, M.H. Wong, F.T. Cheng, Stearic acid coating on magnesium for enhancing corrosion resistance in Hanks' solution, Surf. Coat. Technol 204 (2010) 1823.

[21] Y. Zhu, G. Wu, Y.-H. Zhang, Q. Zhao, Growth and characterization of Mg(OH)2 film on magnesium alloy AZ31, Appl. Surf. Sci. 257 (2011) 6129.

[22] R.K. Gupta, K. Mensah-Darkwa, D. Kumar, Corrosion Protective Conversion Coatings on Magnesium Disks Using a Hydrothermal Technique, J Mater Sci Technol **30 (**2014) 47.

[23] Sara Kaabi Falahieh Asl , Nemeth Sandor, M.J. Tan, Hydrothermally Deposited Protective and Bioactive Coating for Magnesium Alloys for Implant Application,paper in press.

[24] T. Kokubo, Apatite formation on surfaces of ceramics, metals and polymers in body environment, Acta Mater 46 (1998) 2519.

[25] C. Liu, Y. Xin, G. Tang, P.K. Chu, Influence of heat treatment on degradation behavior of bio-degradable die-cast AZ63 magnesium alloy in simulated body fluid, Mater. Sci. Eng., A 456 (2007) 350.

[26] H.X. Wang, S.K. Guan, X. Wang, C.X. Ren, L.G. Wang, In vitro degradation and mechanical integrity of Mg-Zn-Ca alloy coated with Ca-deficient hydroxyapatite by the pulse electrodeposition process, Acta Biomater 6 (2010) 1743.

[27] S. Zhang, F. Cao, L. Chang, J. Zheng, Z. Zhang, J. Zhang, C. Cao, Electrodeposition of high corrosion resistance Cu/Ni–P coating on AZ91D magnesium alloy, Appl. Surf. Sci. 257 (2011) 9213.

[28] J. Fan, X. Qiu, X. Niu, Z. Tian, W. Sun, X. Liu, Y. Li, W. Li, J. Meng, Microstructure, mechanical properties, in vitro degradation and cytotoxicity evaluations of Mg-1.5Y-1.2Zn-0.44Zr alloys for biodegradable metallic implants, Mater. Sci. Eng., C 33 (2013) 2345.

[29] W.A. Badawy, N.H. Hilal, M. El-Rabiee, H. Nady, Electrochemical behavior of Mg and some Mg alloys in aqueous solutions of different pH, Electrochim. Acta 55 (2010) 1880.

[30] S. Creager, 3 - Solvents and Supporting Electrolytes, in: G.Z. Cynthia (Ed.) Handbook of Electrochemistry, Elsevier, Amsterdam, 2007, pp. 57-IV.

[31] Z. Yao, Z. Jiang, F. Wang, Study on corrosion resistance and roughness of micro-plasma oxidation ceramic coatings on Ti alloy by EIS technique, Electrochim. Acta 52 (2007) 4539.

[32] A. Conde, J. de Damborenea, Evaluation of exfoliation susceptibility by means of the electrochemical impedance spectroscopy, Corros. Sci. 42 (2000) 1363.

[33] M. Razavi, M. Fathi, O. Savabi, S. Mohammad Razavi, B. Hashemi Beni, D. Vashaee, L. Tayebi, Controlling the degradation rate of bioactive magnesium implants by electrophoretic deposition of akermanite coating, Ceram. Int. 40 (2014) 3865.

[34] G. Ballerini, U. Bardi, R. Bignucolo, G. Ceraolo, About some corrosion mechanisms of AZ91D magnesium alloy, Corros. Sci 47 (2005) 2173.

[35] Y. Wang, C.S. Lim, C.V. Lim, M.S. Yong, E.K. Teo, L.N. Moh, In vitro degradation behavior of M1A magnesium alloy in protein-containing simulated body fluid, Mater. Sci. Eng., C 31 (2011) 579.

[36] X. Xin-bo, Z. Xie-rong, Z. Chun-li, L. Ping, F. Yun-bo, Influence of hydrothermal temperature on hydroxyapatite coating transformed from monetite on HT-C/C composites by induction heating method, Surf. Coat. Technol 204 (2009) 115.

Figure's caption

Fig.1. a) Open circuit potential curves and b) potentiodynamic curves of uncoated and coated samples for different deposition temperature in SBF solution

Fig.2. Potentiodynamic curves of uncoated and coated samples at 190 °C for different deposition time

Fig.3. Nyquist of uncoated and coated samples in SBF solution (Insert is AZ31 Nyquist graph)

Fig.4. a) Bode phase graph and b) Bode plot graph for uncoated and coated samples in SBF solution

Fig.5. Equivalent circuits for: a) uncoated substrate, b) coated samples at 100 °C, 130 °C and 160 °C and c) coated sample at 190 °C

Fig.6. Mass loss as a function of immersion time in SBF solution for uncoated and coated samples

Fig.7. Photographs of tested samples after 28 days immersion test: a) AZ31 substrate, b) HE100 °C-3hr, c) HE130 °C-3hr, d) HE160 °C-3hr

Fig.8. SEM micrograph of: a)AZ31 substrate, b)HE160 °C-3hr after 28 days immersion in SBF solution

Fig.9. Mg ion release for uncoated and coated sample during immersion in SBF solution

Fig.10. pH change for uncoated and coated sample during immersion in SBF solution

Table1.Potentiodynamic polarization curves parameter derived by the Tafel extrapolation

Sample	j_{corr}(A.cm^{-2})	E_{corr}(V vs. SCE)
AZ31 Substrate	$1.2*10^{-4}$	-1.5
HE100 ºC-3hr	$1.2*10^{-5}$	-1.5
HE130 ºC-3hr	$2.8*10^{-6}$	-1.1
HE160 ºC-3hr	$1.1*10^{-7}$	-0.8
HE190 ºC-3hr	$2.31*10^{-8}$	-0.7
HE190 ºC-2hr	$4.2*10^{-6}$	-0.7
HE190 ºC-1hr	$2.2*10^{-5}$	-1.4

Table2.EIS parameters derived from Impedance spectrums

Sample	R_{ct} (Ω.cm^2)	R_p (Ω.cm^2)	R_{ns} (Ω.cm^2)	|Z| (Ω.cm^2)	C_{dl} (μF/cm^2)	C_f (μF/cm^2)	C_{ns} (nF/cm^2)
AZ31 substrate	47.1	61.49	…	141	20.6	8.2	…
HE100 °C-3hr	…	1981	…	1421	…	3.9	…
HE130 °C-3hr	…	1259.7	…	928.9	…	4.1	…
HE160 °C-3hr	…	4182	…	3305	…	9.6	…
HE190 °C-3hr	…	6478.9	2748	7712	…	12.3	0.58

Table3. Cumulative Mg ion concentration released from the coated and bare substrate

Immersion period (Day)	Mg ion release (ppm/cm^2)			
	AZ31 substrate	HE100 °C-3hr	HE130 °C-3hr	HE160 °C-3hr
2	83.1± 3.6	16.2 ± 1.8	12.8 ± 1.6	11.2 ± 1.8
4	105.8± 3.9	34.6 ± 2.2	27.3 ± 1.6	22.6 ± 2.8
7	115.5 ± 4.3	38.4 ± 3.3	35.5 ± 2.6	32.7 ± 3.2
14	118.6 ± 2.7	115.7 ± 4.3	111.6 ± 3.4	82.5 ± 3.3
21	154.1± 4.6	128.8 ± 3.4	118.3 ± 3.9	101.7 ± 2.9
28	174.9 ± 6.3	141.2 ± 4.9	122.5 ± 3.8	108.0 ± 4.3

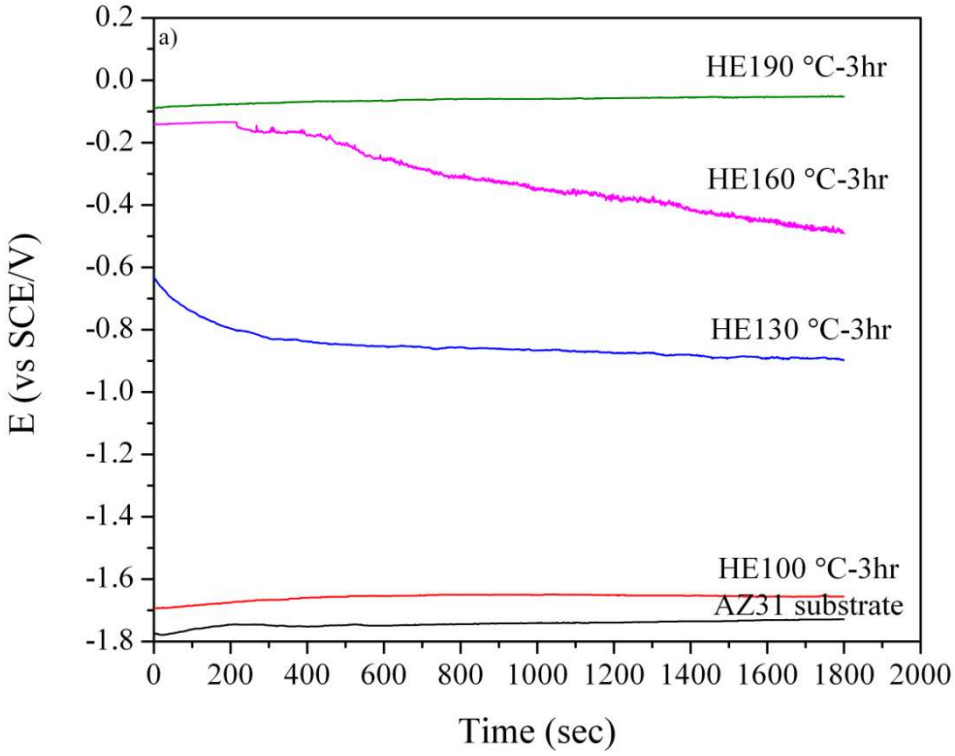
a)
HE190 °C-3hr
HE160 °C-3hr
HE130 °C-3hr
HE100 °C-3hr
AZ31 substrate
E (vs SCE/V)
Time (sec)
0.2
0.0
-0.2
-0.4
-0.6
-0.8
-1.0
-1.2
-1.4
-1.6
-1.8
0
200
400
600
800
1000
1200
1400
1600
1800
2000

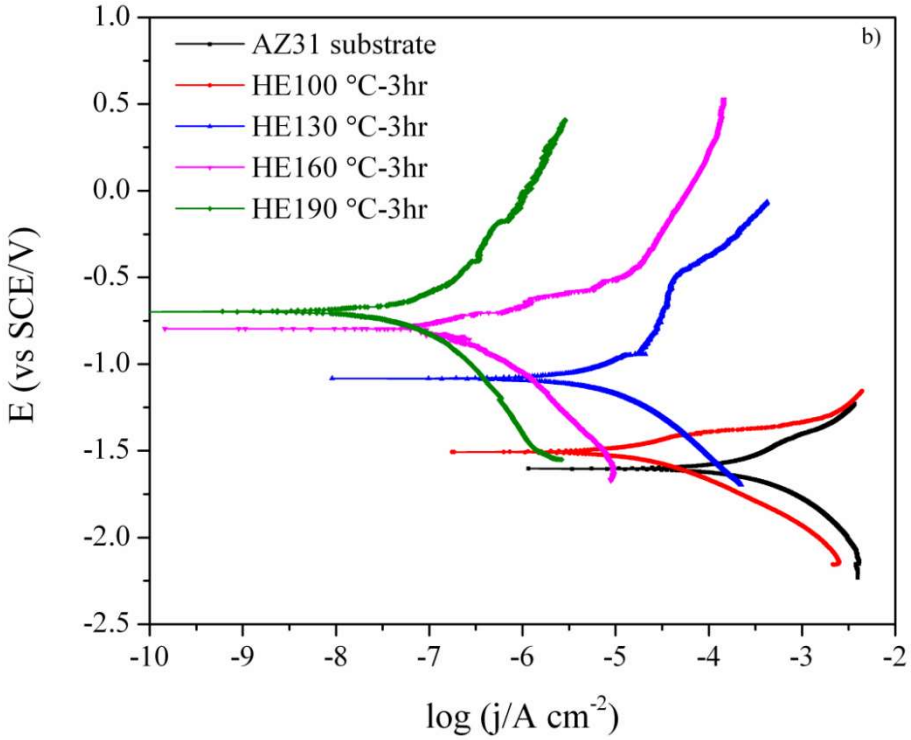
b)
AZ31 substrate
HE100 °C-3hr
HE130 °C-3hr
HE160 °C-3hr
HE190 °C-3hr
E (vs SCE/V)
log (j/A cm-2)
1.0
0.5
0.0
-0.5
-1.0
-1.5
-2.0
-2.5
-10
-9
-8
-7
-6
-5
-4
-3
-2

Fig.1

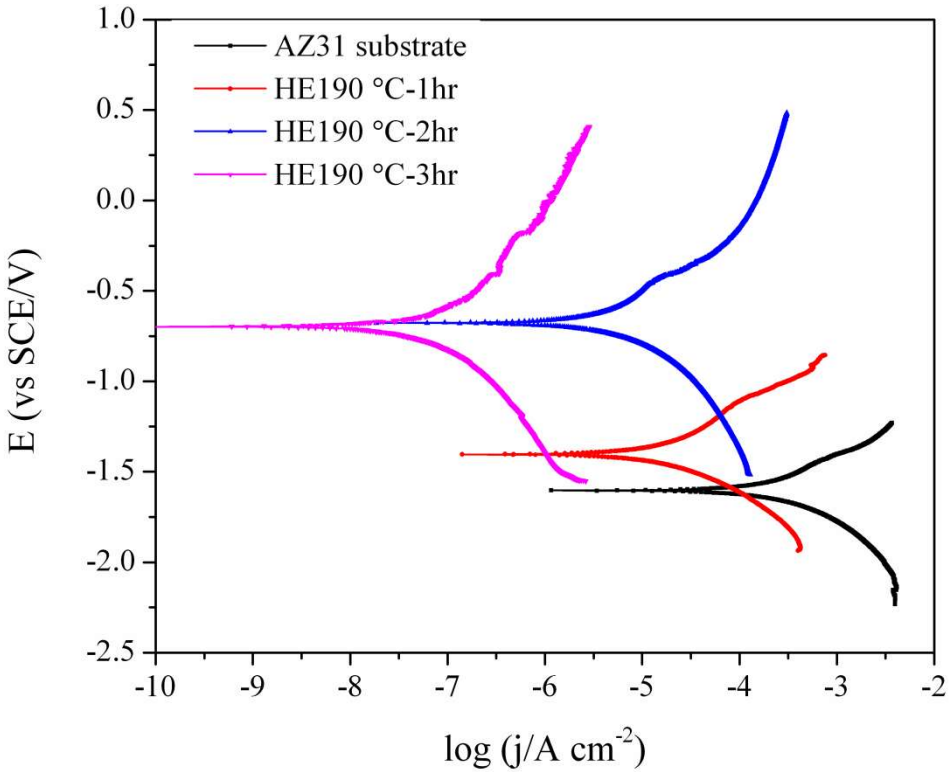
AZ31 substrate
HE190 °C-1hr
HE190 °C-2hr
HE190 °C-3hr
E (vs SCE/V)
log (j/A cm-2)
1.0
0.5
0.0
-0.5
-1.0
-1.5
-2.0
-2.5
-10
-9
-8
-7
-6
-5
-4
-3
-2

Fig.2

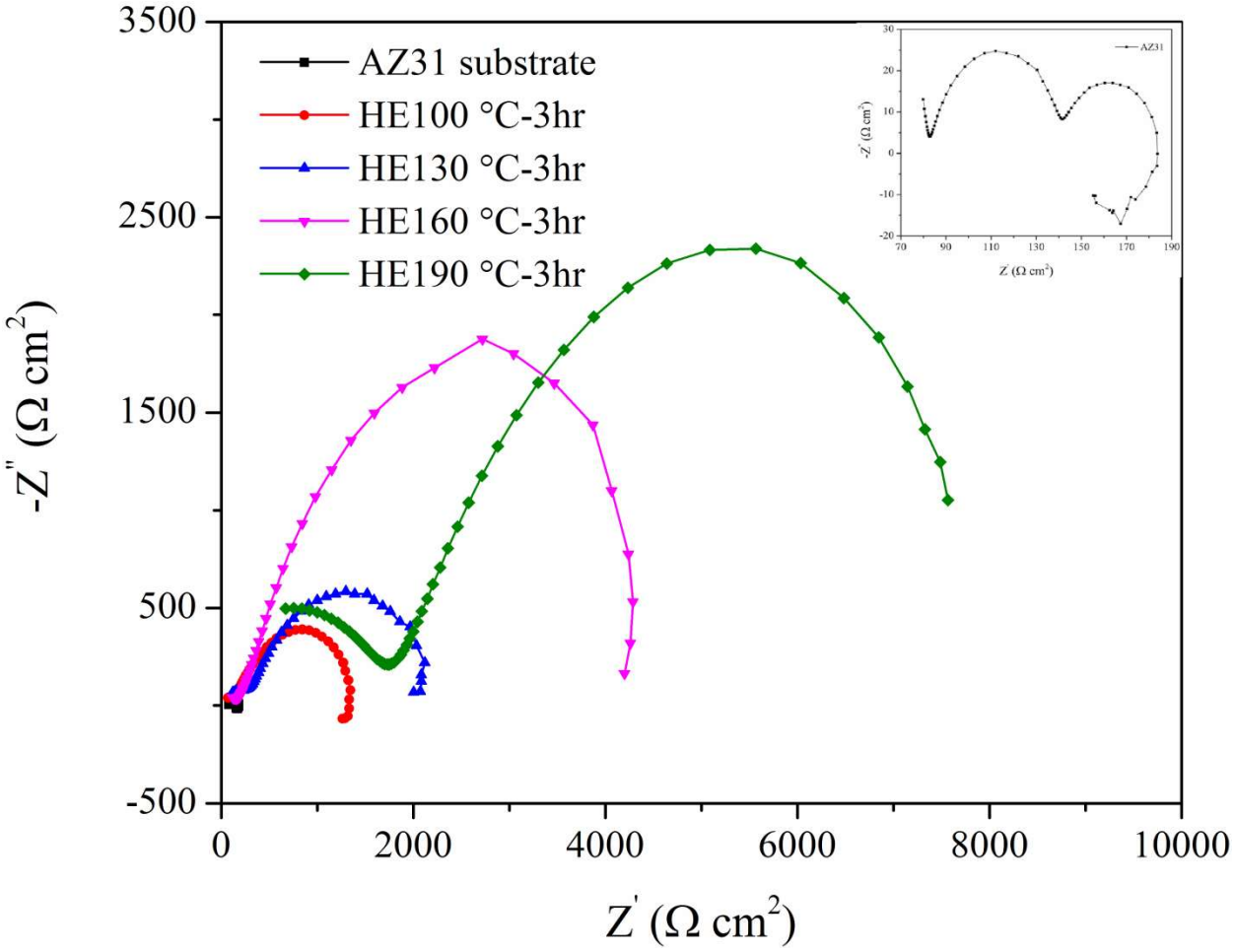
AZ31 substrate
HE100 °C-3hr
HE130 °C-3hr
HE160 °C-3hr
HE190 °C-3hr
-Z'' (Ω cm2)
Z' (Ω cm2)
3500
2500
1500
500
-500
0
2000
4000
6000
8000
10000
AZ31
-Z' (Ω cm2)
Z (Ω cm2)

Fig.3

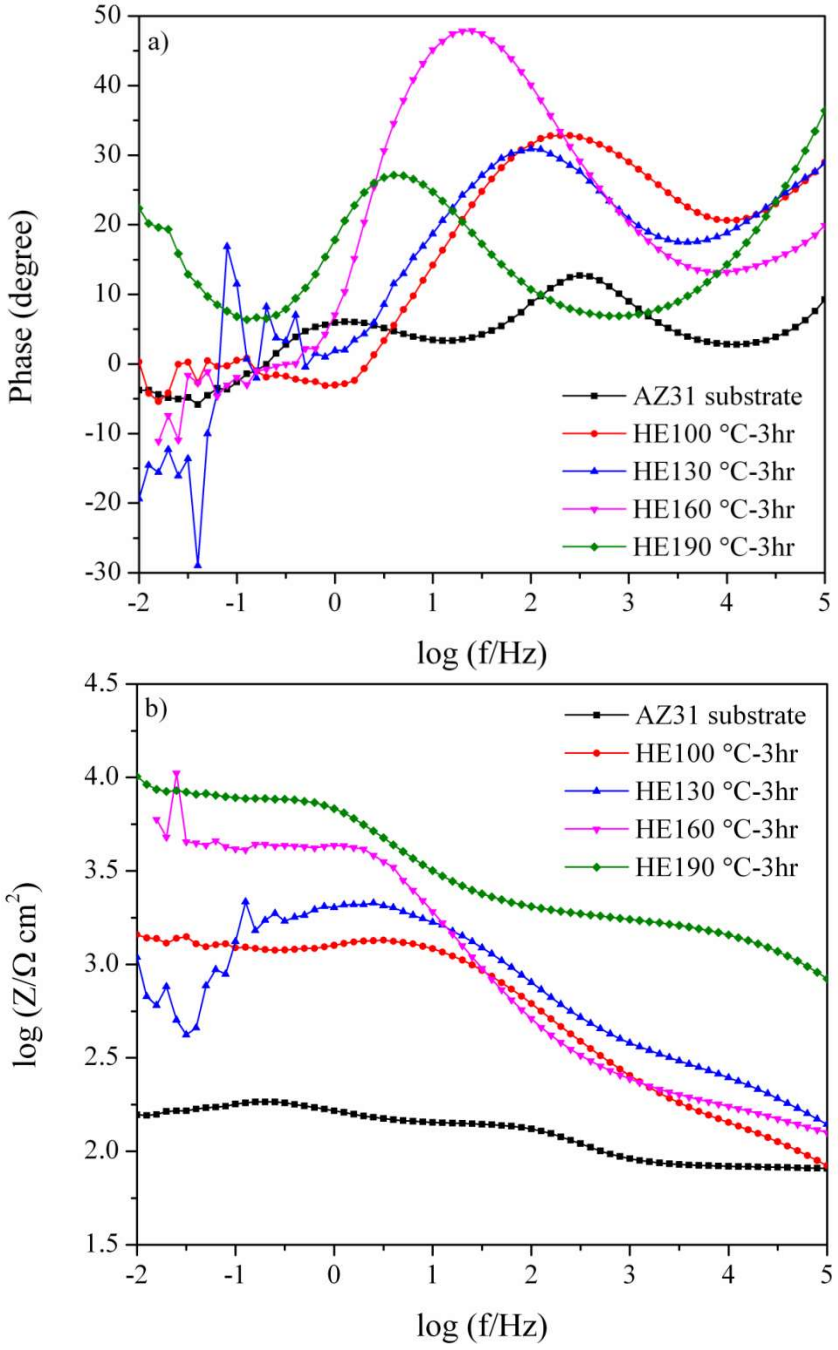
a)
Phase (degree)
log (f/Hz)
AZ31 substrate
HE100 °C-3hr
HE130 °C-3hr
HE160 °C-3hr
HE190 °C-3hr
b)
log (Z/Ω cm^2)
log (f/Hz)
AZ31 substrate
HE100 °C-3hr
HE130 °C-3hr
HE160 °C-3hr
HE190 °C-3hr

Fig.4

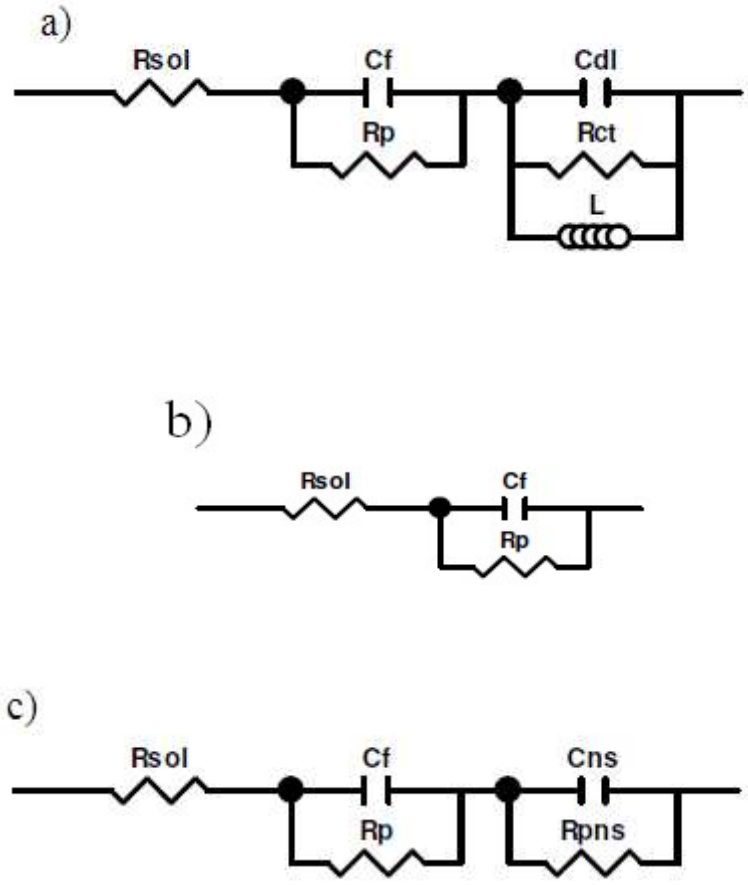

Fig.5

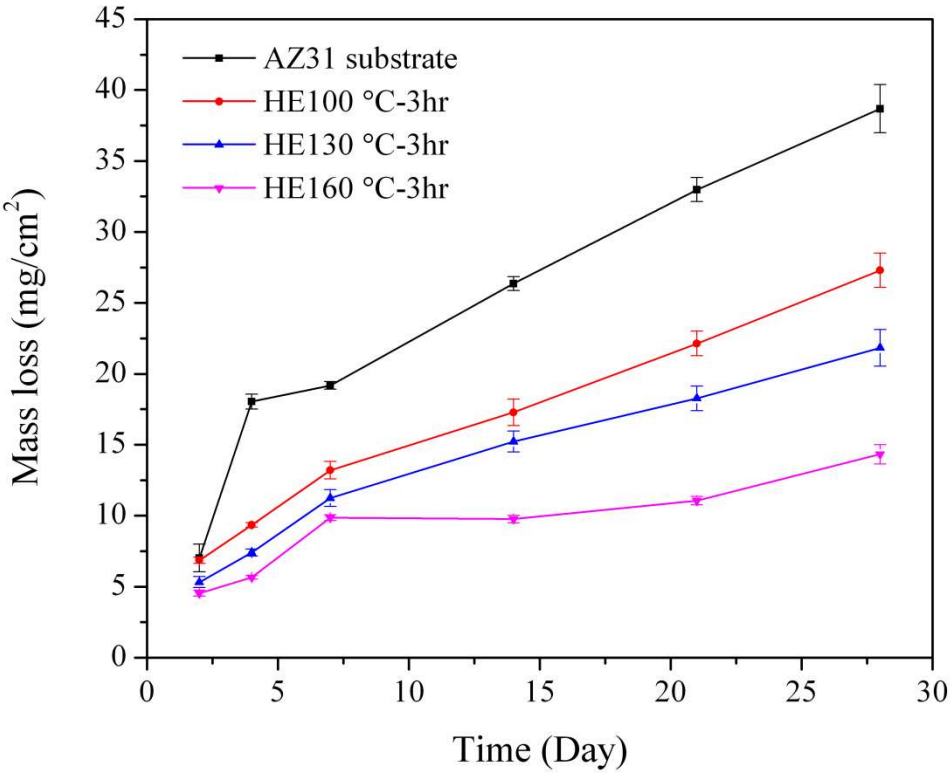
AZ31 substrate
HE100 °C-3hr
HE130 °C-3hr
HE160 °C-3hr
Mass loss (mg/cm^2)
Time (Day)
0
5
10
15
20
25
30
35
40
45

Fig.6

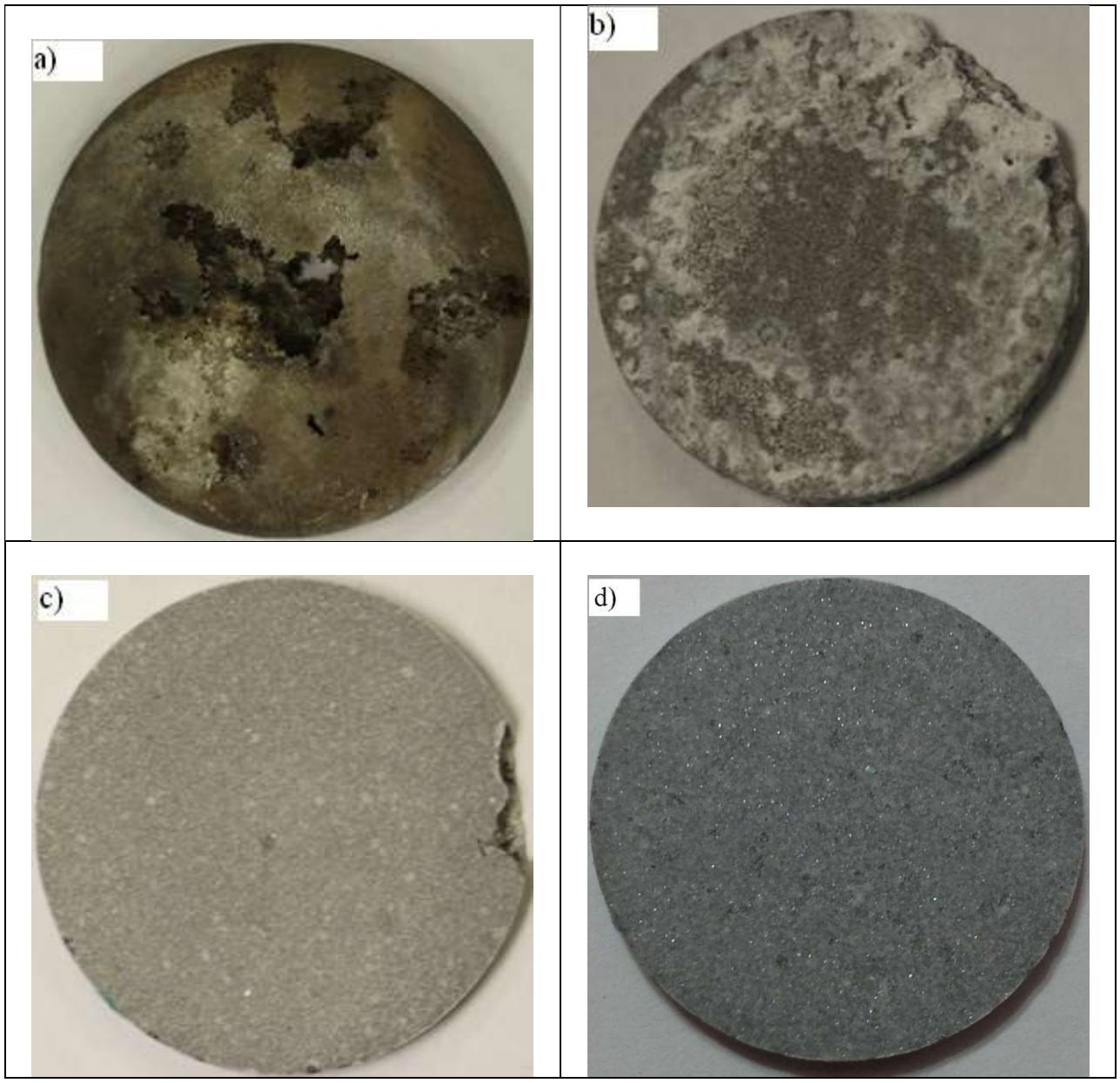

Fig.7

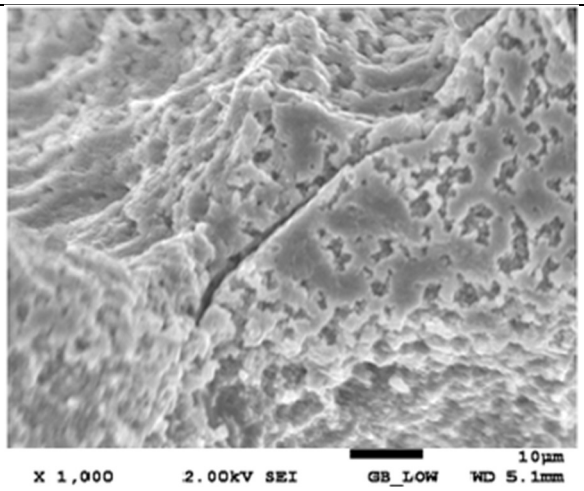
10µm
X 1,000 2.00kV SEI GB_LOW WD 5.1mm

(a)

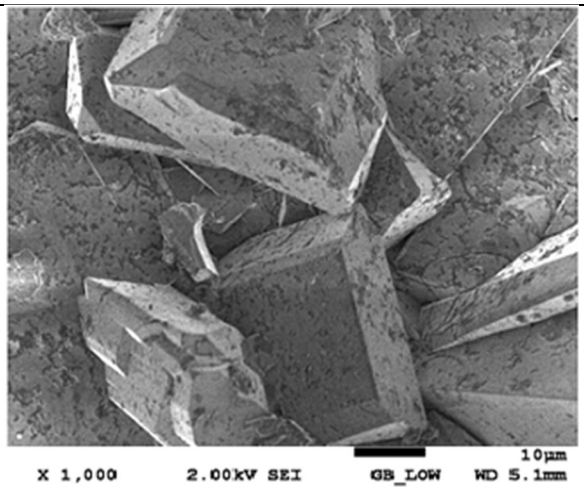
10µm
X 1,000 2.00kV SEI GB_LOW WD 5.1mm

(b)

Fig.8

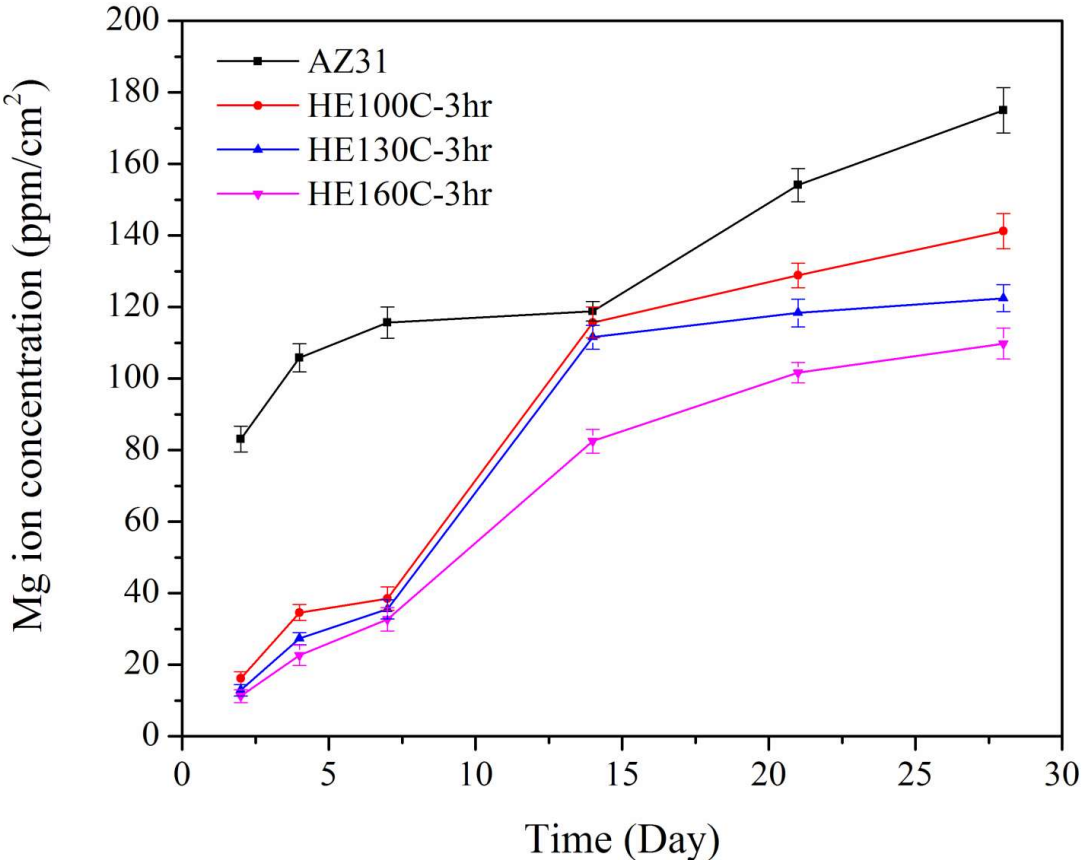
AZ31
HE100C-3hr
HE130C-3hr
HE160C-3hr
Mg ion concentration (ppm/cm^2)
Time (Day)
0
20
40
60
80
100
120
140
160
180
200
0
5
10
15
20
25
30

Fig.9

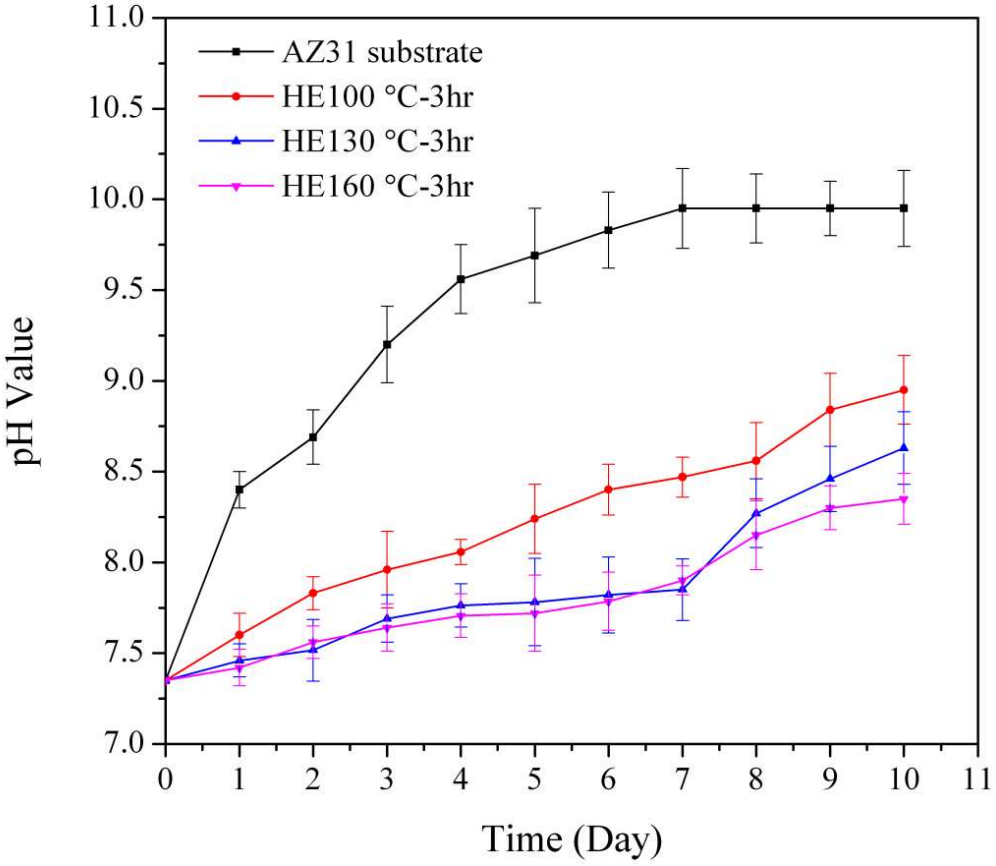
AZ31 substrate
HE100 °C-3hr
HE130 °C-3hr
HE160 °C-3hr
pH Value
Time (Day)
11.0
10.5
10.0
9.5
9.0
8.5
8.0
7.5
7.0
0
1
2
3
4
5
6
7
8
9
10
11

Fig.10